

Many-body effects in transport through a quantum dot

Yukihiro Tanaka and Hiroshi Akera

Department of Engineering Science, Faculty of Engineering, Hokkaido University, Sapporo 060, Japan

(Received 29 March 1995; revised manuscript received 8 September 1995)

Exact many-body eigenstates in a quantum dot formed in double-barrier heterostructures are calculated in the limit of strong confinement, and the nonlinear coherent transport through the states is studied for temperatures larger than their level broadenings. Energy splittings between many-body states due to exchange and correlation effects manifest themselves as small steps which decorate the Coulomb staircase in the current-voltage characteristics, which strongly depends on the number of electrons in the dot. Clear many-body effects are also found in peak heights and peak separations in the Coulomb oscillation of the linear conductance.

I. INTRODUCTION

Quantum dots, artificial atoms fabricated in semiconductor heterostructures,¹ have given a new opportunity to study many-body effects in solid state physics. Different from natural atoms, such artificial atoms can be connected to leads and the obtained current signal is expected to reveal the nature of electron interactions in this system. In this paper many-body effects in such a quantum dot on the transport are studied theoretically.

Transport through a small metallic grain has been investigated extensively and most of the observed phenomena are now well understood in terms of a capacitance associated with a grain.² Because of the small size, the charging energy of a grain associated with the addition of one electron can be much larger than the temperature and produces new features in transport through the grain, such as the Coulomb oscillation, which appears in the conductance as a function of the gate voltage to the grain, and the Coulomb staircase, which is observed in the current-voltage characteristics. In a metallic grain that is much larger than the Fermi wavelength, the charging energy is well described by the capacitance between the grain and leads.

Recently many experiments have been made on the transport through a semiconductor dot,¹ but many phenomena remain unsolved, in particular, those in a very small dot with a few electrons that are fabricated from double-barrier heterostructures.³⁻⁹ A dot made of a semiconductor has larger level separations due to smaller effective mass and is therefore called a quantum dot. Calculations taking into account such quantized energy levels have been made within an approximation, which assumes a constant capacitance between the dot and leads.^{10,11} Although such calculations give a useful guide to analyze many experiments, it is necessary to improve the theory in the following two points to explain experiments on very small dots.

The first point is to go beyond the constant-capacitance model by incorporating the state dependence of the charging energy. Each state has a wave-function profile that is different from state to state and therefore it is necessary to take into account the difference in the charging energy between states when the level quantization is important.^{4,12} In quantitative calculations of the charging energy, it is also important in many cases to take into account the screening of a charge

in the dot by the leads and the gate contact. Such a calculation of the charging energy has been made within the Hartree approximation for a quantum dot defined in a two-dimensional system by split gates, and the obtained result is close to that of the constant-capacitance model because of the large number (from 40 to 70) of electrons in the dot.¹³ The same calculation in small dots is desirable.

The second point is to go beyond the Hartree approximation. It is necessary to include the electron correlation when single-electron energy levels are degenerate, because many-body eigenstates are determined by electron interactions. Such correlation effects are known to be essential in the fractional quantum Hall effect that occurs in discrete, degenerate Landau levels. Recently studies have been extended to a quantum dot in strong magnetic fields, and calculations have been made of its addition spectra¹⁴⁻¹⁶ and of its conductance.¹⁷

The electron correlation plays an important role also in the absence of magnetic field,¹⁸ in particular, in the circular dot in double-barrier heterostructures.^{4,8} The in-plane confining potential of the circular dot is well modeled by a two-dimensional parabolic potential $\frac{1}{2}m^*\omega_0^2(x^2+y^2)$ with m^* the effective mass. This potential produces energy levels with energy $\hbar\omega_0(n+1)$ where $n=0,1,2,\dots$ and the degeneracy of each level is $n+1$ excluding the spin degeneracy. The electron correlation is expected to be important for $n \geq 1$.

The purpose of this paper is to clarify how the current-voltage characteristics is modified in such a system when the exchange and correlation effects are taken into account. To maximize effects of the electron correlation, a quantum limit is considered, in which the level separation $\hbar\omega_0$ is much larger than Coulomb matrix elements and low-energy many-body states are restricted within the subspace of the Hilbert space spanned in the level at the Fermi energy (the levels below the Fermi energy are fully occupied by electrons and inert).

To concentrate on many-body effects within the dot, many complicated aspects in actual systems are simplified. Leads are assumed to be electron reservoirs with a constant density of states and to be connected to the dot by a phenomenological tunneling Hamiltonian. The screening of a charge in the dot by the leads and the gate contact in connection with the first point mentioned above¹³ and the correlation between electrons in the dot and those in the leads such as in the

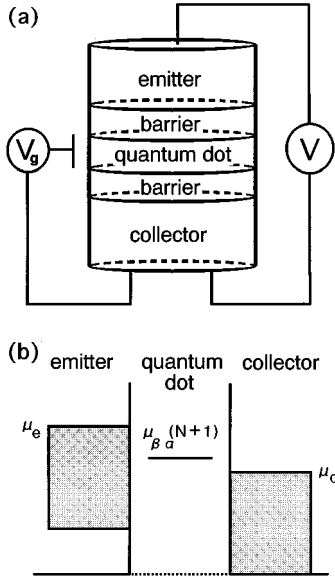


FIG. 1. (a) Schematic of a cylindrical double-barrier structure with a quantum dot formed between barriers. V is the bias voltage and V_g is the gate voltage to control the potential at the dot. (b) Parameters to be used in the calculation. The potential at the dot is fixed and the chemical potential at the emitter and at the collector are varied. $\mu_{\beta\alpha}(N+1) = E_{\beta}(N+1) - E_{\alpha}(N)$ with $E_{\alpha}(N)$ the energy of N -electron state α .

Kondo effect^{20,21} are neglected.

The device, which was used in an experiment⁹ and is considered in this paper, is schematically illustrated in Fig 1(a). The barriers are modulation doped and N electrons are present in the dot in the equilibrium, that is, in the absence of current. The gate contact is attached to control the potential at the dot. By raising the chemical potential of the emitter, an electron in the emitter tunnels through one of states with $N+1$ electrons in the dot [see Fig. 1(b)]. It is assumed here that only one channel through one state is open for a given spin at a given energy and possible interference phenomena,²² which will occur when there are more than one many-body states within the width of the level broadening, are neglected.

This paper is organized as follows. In Sec. II a model of the dot and the leads is given. The quantum limit is introduced in calculating many-body states in the dot and shown to be applicable in some examples. In Sec. III a current formula is derived on the basis of the coherent tunneling through many-body states. In Sec. IV calculated results of the current-voltage characteristics and the conductance, as well as many-body energy spectra in the quantum limit, are given. A comparison with the Hartree-Fock approximation and the Hartree approximation is made to clarify effects of the exchange and correlation. In addition, a comparison of our results with recent experiments is made. In Sec. V the conclusion is given.

II. HAMILTONIAN

Our model Hamiltonian consists of the unperturbed Hamiltonian of the dot, the emitter, and the collector, H_0 , and the tunneling Hamiltonian, H_t :

$$H = H_0 + H_t, \quad (1)$$

with

$$H_0 = H_d + H_e + H_c. \quad (2)$$

The potential in the dot formed in double-barrier heterostructures is well approximated by the sum of the barrier potential (the z axis is along the growth direction) and the parabolic in-plane potential by the electrostatic confinement, the latter being given by $m^* \omega_0^2 r^2 / 2$ with m^* the effective mass and $r = (x^2 + y^2)^{1/2}$. We consider only the lowest level associated with the motion along the z axis and measure energies from this level. Single-particle states are then represented by three quantum numbers: the principal quantum number n ($n=0, 1, 2, \dots$), the orbital angular momentum m ($m=0, \pm 1, \pm 2, \dots$), and the spin σ ($\sigma = \pm 1$). The eigenfunction of the in-plane part is

$$\phi_{nm}(r, \theta) = (2\pi)^{-1/2} \exp(-im\theta) \chi_{jm} \left(\frac{r}{l_0} \right), \quad (3)$$

with

$$\chi_{jm}(\rho) = \frac{\sqrt{2}}{l_0} \left(\frac{j!}{(j+|m|)!} \right)^{1/2} \exp\left(-\frac{\rho^2}{2}\right) \rho^{|m|} L_j^{|m|}(\rho^2), \quad (4)$$

and the corresponding eigenenergy is

$$\varepsilon_n = \hbar \omega_0 (n+1). \quad (5)$$

Here $l_0 = (\hbar/m^* \omega_0)^{1/2}$ and $L_j^m(x)$ is the Laguerre polynomial. Since $j = (n - |m|)/2$ takes non-negative integers, the allowed value of m at each n is $m=0$ for $n=0$, $m = \pm 1$ for $n=1$, $m=0, \pm 2$ for $n=2$, and so on. The degeneracy of the n th level is $n+1$. The extent of the wave function in the z direction is assumed to be negligible compared with that of the in-plane wave function, l_0 .

The Hamiltonian of the isolated dot in the second-quantization form is then expressed by

$$H_d = \sum_{nm\sigma} \varepsilon_n c_{nm\sigma}^\dagger c_{nm\sigma} + \frac{1}{2} \sum_{n_1 m_1 n_2 m_2 n_3 m_3 n_4 m_4 \sigma'} U_{n_1 m_1 n_2 m_2 n_3 m_3 n_4 m_4} \times c_{n_1 m_1}^\dagger c_{n_2 m_2}^\dagger c_{n_3 m_3} c_{n_4 m_4} \sigma', \quad (6)$$

with

$$U_{n_1 m_1 n_2 m_2 n_3 m_3 n_4 m_4} = \int d\mathbf{r} \int d\mathbf{r}' \phi_{n_1 m_1}^*(\mathbf{r}) \phi_{n_2 m_2}^*(\mathbf{r}') \times \frac{e^2}{\varepsilon |\mathbf{r} - \mathbf{r}'|} \phi_{n_3 m_3}(\mathbf{r}') \phi_{n_4 m_4}(\mathbf{r}), \quad (7)$$

$\mathbf{r} = (x, y)$, and ε the dielectric constant. Two characteristic energy scales, the level spacing $\hbar \omega_0$, and the typical Coulomb energy $e^2/\varepsilon l_0$ are plotted as a function of l_0 in Fig. 2. For l_0 smaller than the effective Bohr radius, $\hbar \omega_0$ is larger than $e^2/\varepsilon l_0$. In this paper we consider the quantum limit of $\hbar \omega_0 \gg e^2/\varepsilon l_0$ and level mixings due to off-diagonal Coulomb matrix elements are neglected. The applicability of the quan-

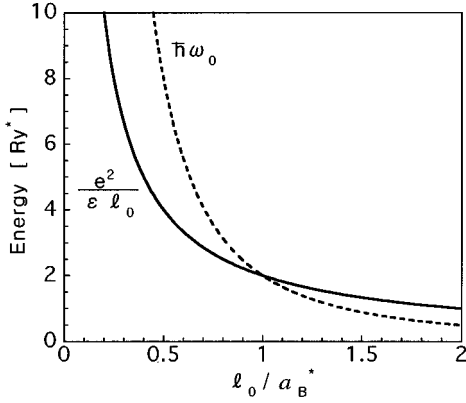


FIG. 2. Level separation $\hbar\omega_0$ and typical Coulomb energy $e^2/\epsilon l_0$ as a function of l_0 in units of $\text{Ry}^* = m^*e^4/2\hbar^2\epsilon^2$. $a_B^* = \hbar^2\epsilon/m^*e^2$ is the effective Bohr radius. $a_B^* = 104 \text{ \AA}$ in GaAs, 296 \AA in InAs, 631 \AA in InSb and $\text{Ry}^* = 5.29 \text{ meV}$ in GaAs, 1.67 meV in InAs, 0.638 meV in InSb.

tum limit, or the approximation to neglect level mixings, is examined in detail in the Appendix. It is shown there that in dots in the GaAs well, which have been reported so far, $\hbar\omega_0$ and $e^2/\epsilon l_0$ are comparable and the quantum limit is not applicable. However, it is also shown there that the quantum limit may be applicable in a dot formed in other materials with smaller effective mass, such as InSb. Label the level at the Fermi level as n_F . In the quantum limit the levels below n_F are fully occupied by electrons and those above n_F are empty and the Hamiltonian in this limit is expressed (omitting the subscript n_F when possible) by

$$H_d(n_F) = \sum_{m\sigma} (\epsilon_{n_F} + u_{n_F m}) c_{m\sigma}^\dagger c_{m\sigma} + \frac{1}{2} \sum_{m_1 m_2 m_3 m_4 \sigma \sigma'} U_{m_1 m_2 m_3 m_4} c_{m_1 \sigma}^\dagger c_{m_2 \sigma'}^\dagger c_{m_3 \sigma} c_{m_4 \sigma'}, \quad (8)$$

with

$$u_{n_F m} = \sum_{n' < n_F, m'} (2U_{n_F m n' m'} - U_{n_F m n' m'}). \quad (9)$$

Here $u_{n_F m}$ takes into account the interaction between an electron in the n_F th level with those in the lower filled levels in the Hartree-Fock approximations. Since the system we consider has the rotational symmetry around the z axis and in the spin space, many-body eigenstates are labeled by the total orbital angular momentum, the total spin, and its z component.

The wave function and the energy in the Hartree-Fock approximation is given by $|\text{HF}\rangle = \prod_i c_{n_F m_i \sigma_i}^\dagger |0\rangle$ and $\langle \text{HF} | H_d(n_F) | \text{HF} \rangle$ with $|0\rangle$ representing the filled levels up to the $(n_F - 1)$ th level. Exchange terms in $\langle \text{HF} | H_d(n_F) | \text{HF} \rangle$ and in $u_{n_F m}$ are dropped in the evaluation of the energy in the Hartree approximation.

The Hamiltonian of lead l ($l = e$ for the emitter and $l = c$ for the collector) is

$$H_l = \sum_{k\sigma} \epsilon_{lk} a_{lk\sigma}^\dagger a_{lk\sigma}, \quad (10)$$

where k represents a continuous quantum number characterizing a state in a lead.

Finally the tunneling Hamiltonian is

$$H_t = \sum_{lkm\sigma} t_l (c_{n_F m \sigma}^\dagger a_{lk\sigma} + \text{H.c.}). \quad (11)$$

Here we have assumed that matrix elements are independent of states involved. In particular this Hamiltonian does not conserve the orbital angular momentum, which might be the case when impurities are present in barriers and leads.

III. CURRENT FORMULA

Instead of using the general current formula in terms of the Keldysh-Green function,²³ in this paper we take a simpler approach, which is valid except in the regime of the Kondo effect at very low temperatures. We assume that the thermal energy $k_B T$ is much larger than the level broadening of many-body states in the dot and obtain the same current formula as that derived from the master equation.^{10,11} This agreement was previously proved in the linear transport regime,²³ but not in the nonlinear regime we consider in this paper, although it might be expected in the view of the thermally broadened resonant-tunneling current peak.^{10,11} We emphasize here that our theory assumes no inelastic processes in the dot.

We calculate the current through the dot by treating H_t as a perturbation and assume that the two leads stay in the equilibrium. In this paper we only consider the tunneling of a single electron at a time and therefore the transition is exclusively between states with N electrons in the n_F th level and those with $N+1$ electrons. This is the case when the bias voltage is not very high or when the barrier in the collector side is much more transparent than that in the emitter side and the probability of having $N+2$ electrons and more is negligible.

As an illustration, we first consider the case where the transition is possible only between a single N -electron state, α , and a single $(N+1)$ -electron state, β . Consider the following transition. The initial state is $|\alpha\rangle|i\rangle$ in which the $ek\sigma$ state is occupied and the $cq\sigma$ state is vacant, $|i\rangle$ representing the occupation of levels in the two leads. The intermediate state is $|\beta\rangle|m\rangle$ with $|m\rangle = a_{ek\sigma}|i\rangle$. The conservation of the total spin requires that $\sigma = 2(S_\beta - S_\alpha)$. The final state is $|\alpha\rangle|f\rangle$ with $|f\rangle = a_{cq\sigma}^\dagger a_{ek\sigma}|i\rangle$. The transition rate is given by

$$W(\alpha f | \alpha i) = \frac{2\pi}{\hbar} |\langle \alpha f | \hat{T} | \alpha i \rangle|^2 \delta(E_{\alpha i} - E_{\alpha f}), \quad (12)$$

with

$$\hat{T} = H_t + H_t g H_t + H_t g H_t g H_t + \dots \quad (13)$$

The unperturbed Green's function is given by $g = 1/(E - H_0 + i\eta)$ with η the positive infinitesimal and $E = E_{\alpha i} = E_{\alpha f}$. In the evaluation of the matrix element of \hat{T} , we take into account only terms corresponding to pro-

cesses passing through $|\beta\rangle|m\rangle$ as frequently as possible, which are the most important when $E_{\alpha i} \sim E_{\beta m}$. The transition matrix element is then calculated to be

$$\langle \alpha f | \hat{T} | \alpha i \rangle = \frac{\langle \alpha f | H_t | \beta m \rangle \langle \beta m | H_t | \alpha i \rangle}{E - E_{\beta m} - \Sigma_{\beta m}}, \quad (14)$$

with

$$\Sigma_{\beta m} = \sum_j |\langle \beta m | H_t | \alpha j \rangle|^2 \langle \alpha j | g | \alpha j \rangle \quad (15)$$

and $|j\rangle = a_{l\rho\sigma}^\dagger a_{ek\sigma} |i\rangle$. The real part of the self-energy $\Sigma_{\beta m}$ gives unimportant energy shift and is neglected here. Its imaginary part at $E = E_{\beta m}$ is given by $-\Gamma(\alpha|\beta)/2$ with²⁴

$$\Gamma(\alpha|\beta) = 2\pi M_{\beta\alpha} \sum_l t_l^2 D_l [1 - f_l(\mu_{\beta\alpha})], \quad (16)$$

where $M_{\beta\alpha} = |\langle \alpha | c_{m\sigma} | \beta \rangle|^2$ with m the difference of the total angular momentum $M_\beta - M_\alpha$, $\mu_{\beta\alpha} = E_\beta - E_\alpha$, and D_l and f_l are the density of states per spin and the Fermi distribution function, respectively, of lead l .

The current associated with the tunneling of electrons from the emitter to the collector is

$$I_{e \rightarrow c} = -e P_\alpha \sum_i P_i \sum_f n_{ek\sigma}(i) [1 - n_{cq\sigma}(i)] W(\alpha f | \alpha i), \quad (17)$$

where $n_{ek\sigma}(i)$ is 1 if the $ek\sigma$ state is occupied, and 0 if vacant, and P_i is the statistical probability of finding i state. P_α is the probability of finding α state and $P_\alpha + P_\beta = 1$. Due to the equilibrium in each of the leads, $\sum_i P_i n_{ek\sigma}(i) \times [1 - n_{cq\sigma}(i)] = f_e(\epsilon_{ek}) [1 - f_c(\epsilon_{cq})]$. Because $\Gamma(\alpha|\beta) \ll k_B T$, we obtain the total current

$$\begin{aligned} I &= I_{e \rightarrow c} - I_{c \rightarrow e} \\ &= -(e/\hbar) [\Gamma_c(\alpha|\beta) \Gamma_e(\beta|\alpha) \\ &\quad - \Gamma_e(\alpha|\beta) \Gamma_c(\beta|\alpha)] P_\alpha / \Gamma(\alpha|\beta), \end{aligned} \quad (18)$$

with

$$\Gamma_l(\alpha|\beta) = 2\pi M_{\beta\alpha} t_l^2 D_l [1 - f_l(\mu_{\beta\alpha})], \quad (19)$$

$$\Gamma_l(\beta|\alpha) = 2\pi M_{\beta\alpha} t_l^2 D_l f_l(\mu_{\beta\alpha}). \quad (20)$$

To obtain P_α we consider an eigenstate of the total Hamiltonian H . Suppose the system is initially in an eigenstate of H_0 with energy E , $|\alpha\rangle|i\rangle$, in which a state $lk\sigma$ is occupied. The eigenstate of H is then

$$|\psi_i\rangle = |\alpha i\rangle + g H_t |\psi_i\rangle = (1 + g H_t + g H_t g H_t + \dots) |\alpha i\rangle. \quad (21)$$

The probability of finding the system in $|\beta\rangle|m\rangle$ with $|m\rangle = a_{lk\sigma} |i\rangle$ is $|\langle \beta m | \psi_i \rangle|^2$, and $P_\beta = 1 - P_\alpha$ is given by

$$P_\beta = P_\alpha \sum_i P_i \sum_{lk} n_{lk\sigma}(i) |\langle \beta m | \psi_i \rangle|^2 = \Gamma(\beta|\alpha) P_\alpha / \Gamma(\alpha|\beta), \quad (22)$$

with $\Gamma(\beta|\alpha) = \sum_l \Gamma_l(\beta|\alpha)$. Then P_α is obtained and the current is given by

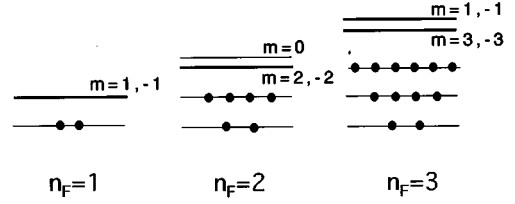


FIG. 3. One-electron energy level when the Fermi level is at the n_F th level. m is the angular-momentum quantum number. The energy due to the Coulomb interaction with electrons in the lower level, $u_{n_F m}$, is $u_{1,1} = 1.567$, $u_{2,2} = 3.936$, $u_{2,0} - u_{2,2} = 0.176$, $u_{3,3} = 6.936$, $u_{3,1} - u_{3,3} = 0.282$ in units of $e^2/\epsilon l_0$ in the Hartree-Fock approximation and $u_{1,1} = 1.880$, $u_{2,2} = 4.504$, $u_{2,0} - u_{2,2} = 0.118$, $u_{3,3} = 7.718$, $u_{3,1} = 0.201$ in the Hartree approximation.

$$I = -\frac{e}{\hbar} M_{\alpha\beta} \frac{\gamma_e \gamma_c}{\gamma_e + \gamma_c} [f_e(\mu_{\beta\alpha}) - f_c(\mu_{\beta\alpha})], \quad (23)$$

with $\gamma_l = 2\pi t_l^2 D_l$.

The generalization of this current formula to cases with many α states and many β states is straightforward, if tunnelings through different β states do not interfere quantum mechanically, that is, when $|\mu_{\beta\alpha} - \mu_{\beta'\alpha}|$ is much larger than the level broadening. The current given by $I = \sum_{\alpha\alpha'} (I_{e\alpha \rightarrow c\alpha'} - I_{c\alpha \rightarrow e\alpha'})$ is

$$\begin{aligned} I &= -(e/\hbar) \sum_\beta \left[\sum_{\alpha'} \Gamma_c(\alpha'|\beta) \sum_\alpha \Gamma_e(\beta|\alpha) P_\alpha \right. \\ &\quad \left. - \sum_{\alpha'} \Gamma_e(\alpha'|\beta) \sum_\alpha \Gamma_c(\beta|\alpha) P_\alpha \right] / \sum_\alpha \Gamma(\alpha|\beta) \end{aligned} \quad (24)$$

$$= -\frac{e}{\hbar} \sum_{\alpha\beta} [\Gamma_e(\beta|\alpha) P_\alpha - \Gamma_c(\alpha|\beta) P_\beta]. \quad (25)$$

In the last equality we have used $\sum_\alpha \Gamma(\alpha|\beta) P_\beta = \sum_\alpha \Gamma(\beta|\alpha) P_\alpha$, which is the generalization of Eq. (22). Ratios between P_α 's are obtained from transition rates between α 's, which are given by

$$W(\alpha'|\alpha) = \frac{1}{\hbar} \sum_\beta \Gamma(\alpha'|\beta) \Gamma(\beta|\alpha) / \sum_\alpha \Gamma(\alpha|\beta). \quad (26)$$

The detailed balance gives

$$\sum_{\alpha'} W(\alpha'|\alpha) P_\alpha = \sum_{\alpha'} W(\alpha|\alpha') P_{\alpha'}. \quad (27)$$

The obtained formula coincides exactly with that from the master equation.

IV. RESULTS

A. Many-body eigenstates

Single-particle energy levels are shown in Fig. 3 when n_F , the level index at the Fermi energy, is 1, 2, and 3. The degeneracy present in the parabolic potential is lifted due to $u_{n_F m}$ in Eq. (8), interactions with electrons in the lower lev-

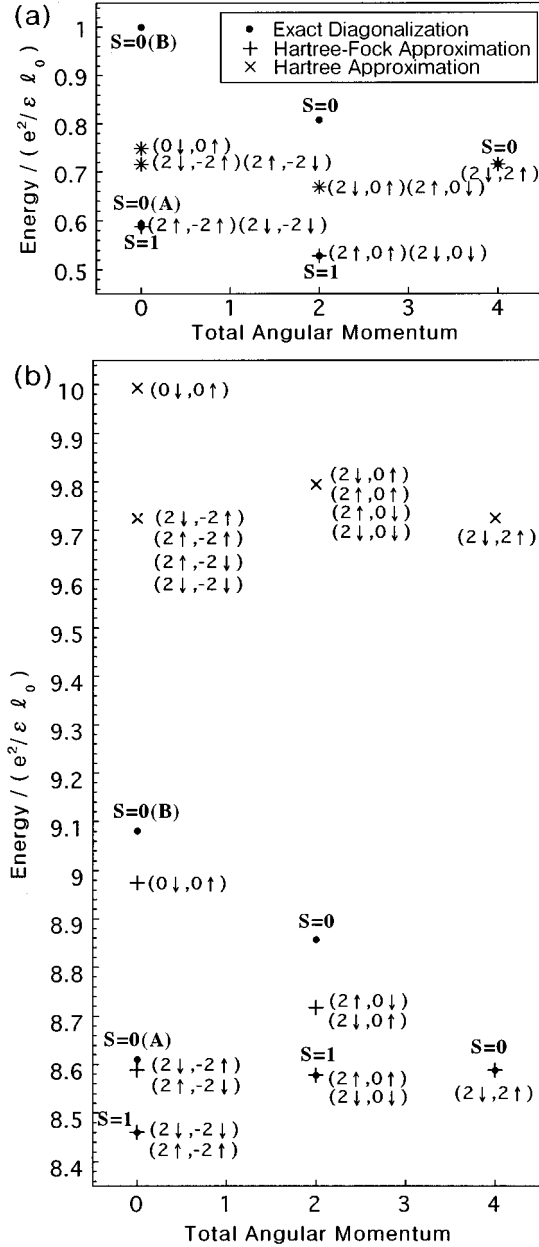


FIG. 4. Two-electron eigenenergies at $n_F=2$ (a) without $u_{n_{Fm}}$ and (b) with $u_{n_{Fm}}$ considered, measured from $2\epsilon_{n_F}$. S is the total spin in the exact-diagonalization result. Two $S=0$ states with the total angular momentum zero are labeled A and B. Electron configuration is designated for the Hartree-Fock result [also for the Hartree result in (b)]. Eigenenergies at negative total angular momentum $-M$ are the same as those at M .

els, when n_F is larger than 1. The dominant electrostatic contribution in $u_{n_{Fm}}$ produces a potential that is the highest at the center, that is at $m=0$.

Two-electron energy levels at $n_F=2$ are shown in Fig. 4. In Fig. 4(a) it is assumed that $u_{n_{Fm}}$ is absent hypothetically to compare with results in Fig. 4(b) in which $u_{n_{Fm}}$ is considered. In each case, results are compared between the exact diagonalization, the Hartree-Fock approximation, and the Hartree approximation. When $u_{n_{Fm}}$ is neglected [Fig. 4(a)], energy splittings present in the Hartree approximation are

due to the difference in the Coulomb interaction between different electron configurations. In the other two calculations, exchange and correlation effects are important in increasing the splittings. A remarkable correlation effect appears in the splitting between two $S=0$ states at the total angular momentum zero in the exact diagonalization. When $u_{n_{Fm}}$ is considered [Fig. 4(b)], however, the difference between the exact diagonalization and the Hartree-Fock approximation is reduced considerably because the degeneracy of single-particle levels is lifted.

B. Nonlinear transport

In this section calculated current-voltage characteristics are presented in the three approximations to clarify the importance of exchange and correlation effects. In most cases results are given with and without $u_{n_{Fm}}$ taken into account to clarify effects of degeneracy. The thermal energy $k_B T$ is much lower than the charging energy, or $e^2/\epsilon \ell_0$ and much higher than the level broadening due to the tunneling.

In the experiment (see Fig. 1), the bias voltage V and the gate voltage V_g are controlled and the potential, say, at the collector V_c is set to zero by connecting it to the ground.⁹ Theoretically, however, it is more convenient to choose another set of parameters, the chemical potential μ_e at the emitter, μ_c at the collector, and the potential V_d at the dot, and to set V_d grounded. In all the figures in this paper, the current is plotted as a function of μ_e at a fixed μ_c .

Several experiments have been made on asymmetric double-barrier structures,^{4,7,8} which have two barriers with different thicknesses, and most calculations in this paper are made on devices in which the barrier in the collector side is thinner than that in the emitter side so that $\gamma_c \gg \gamma_e$. In such a device geometry the dot is approximately in equilibrium with the collector, and the number of electrons changes very little in raising μ_e . This enables us to study transport through excited many-body states as well as the ground state. If $\gamma_e \gg \gamma_c$, on the other hand, the dot is approximately in equilibrium with the emitter and only transport through the ground state appears in the current-voltage characteristics as a function of μ_e .

The saturation current in the limit of large μ_e , which is obtained from Eq. (25), is

$$I_0 = -\frac{e}{\hbar} \gamma_e N_h \sum_{\alpha} P_{\alpha}, \quad (28)$$

with $N_h = 2(n_F + 1) - N$ the number of holes, since $f_e(\mu_{\beta\alpha}) = 1$ at large μ_e and $\sum_{\beta} M_{\beta\alpha} = N_h$. If μ_c and $k_B T$ are low enough to make $f_c(\mu_{\beta\alpha})$ negligible,

$$I_0 = -\frac{e}{\hbar} \frac{N_h \gamma_e (N+1) \gamma_c}{N_h \gamma_e + (N+1) \gamma_c}. \quad (29)$$

In the following the current is plotted in units of I_0 .

The current at zero temperature in the exact diagonalization is plotted as a function of μ_e in Fig. 5(a) when $u_{n_{Fm}}$ is neglected and in Fig. 5(b) when $u_{n_{Fm}}$ is considered at $\gamma_c/\gamma_e = 100$. At low μ_e the second level ($n_F=2$) is occupied by one electron. Above a threshold value of μ_e , the current starts to flow because a channel through a two-

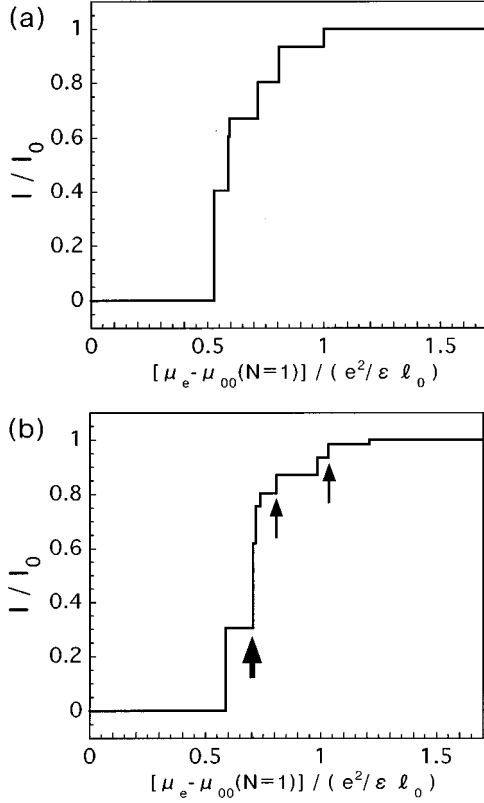


FIG. 5. Current as a function of μ_e in the exact diagonalization at zero temperature, $\gamma_c/\gamma_e=100$, and $n_F=2$ (a) without $u_{n_{Fm}}$ and (b) with $u_{n_{Fm}}$. The current is due to the transition between $N=1$ and $N+1$ electrons in the dot. $I_0 = -(e/\hbar)N_h\gamma_e(N+1)\gamma_c/[N_h\gamma_e + (N+1)\gamma_c]$ with $N_h=2n_F+2-N$ and $\mu_{00}(N)$ is $\mu_{\beta\alpha}$ in which α and β are the ground states with N and $N+1$ electrons, respectively. μ_c is fixed at $\mu_{00}(N=1)+0.1e^2/\epsilon l_0$.

electron state in the n_F -th level is open. There is clear correspondence between current steps here and two-electron levels in Fig. 4. When $u_{n_{Fm}}$ is considered, tunnelings from the excited single-particle level ($m=0$ at $n_F=2$ in Fig. 3) appear at different chemical potentials, which are marked by arrows in Fig. 5(b). At the step onset marked by a thick arrow, the excited single-particle level starts to be populated due to the transition through the two-electron state with $S=1$ at the total angular momentum two, and two channels from the excited single-particle level become open at this chemical potential. Heights of steps in Fig. 5(a) have simple ratios of 6:3:1:2:2:1, reflecting the degeneracy of two-electron levels,²⁵ but there is no such simple relation in Fig. 5(b) due to the splitting in single-particle levels.

An example of the dependence on γ_c/γ_e is presented in Fig. 6 for $n_F=1$ at nonzero temperature. This clearly shows that tunnelings through excited states are more clearly seen at larger γ_c/γ_e . All of the results shown below are at $\gamma_c/\gamma_e=100$.

There are only small dependences on μ_c at low temperatures in the region of $\mu_{00}(N) < \mu_c < \mu_{00}(N+1)$. At large μ_c within this region, some of high-energy excited states with N electrons in the dot are never populated ($P_\alpha=0$ for such states). Nevertheless the current-voltage characteristics do not change much at large γ_c/γ_e . In particular the saturat-

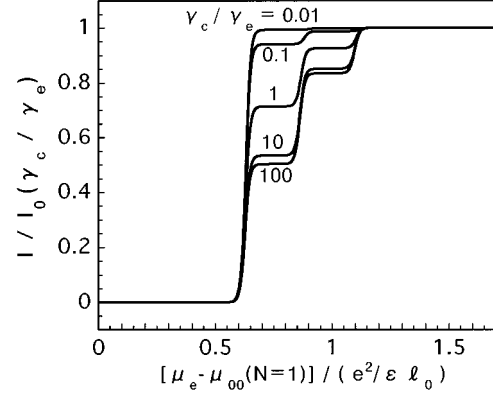


FIG. 6. γ_c/γ_e dependence at $k_B T=0.01e^2/\epsilon l_0$ and $n_F=1$. The current is due to the transition between $N=1$ and $N+1$. Note that I_0 depends on γ_c/γ_e .

tion current at large μ_e is independent of the number of N -electron states participating the transport, since $\sum_\alpha P_\alpha=1$ in Eq. (28) in the limit of large γ_c/γ_e .

A comparison between the exact diagonalization, the Hartree-Fock approximation, and the Hartree approximation is given in Fig. 7(a) when $u_{n_{Fm}}$ is neglected and in Fig. 7(b) when $u_{n_{Fm}}$ is considered. The temperature is $k_B T=0.02e^2/\epsilon l_0$. In Fig. 7(a), compared with the Hartree result, the Hartree-Fock result has current signal at lower chemical potentials due to the exchange effect and has a less steep increase of the current. The exact-diagonalization result has

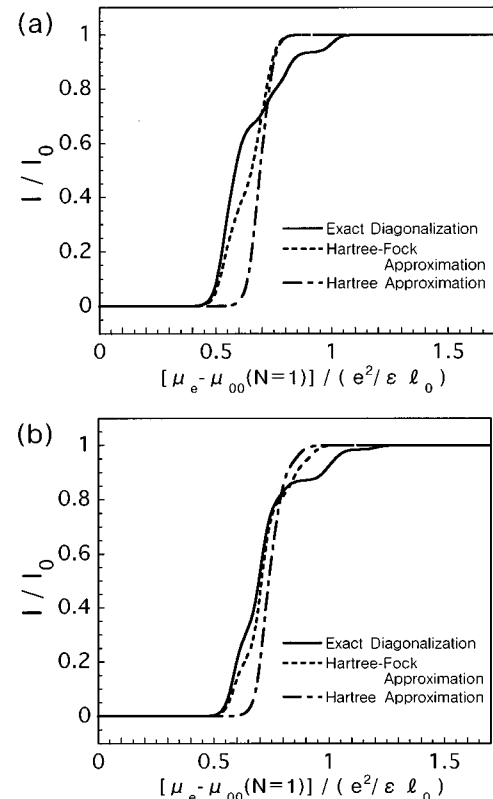


FIG. 7. Comparison with approximate calculations at $n_F=2$ (a) without $u_{n_{Fm}}$ and (b) with $u_{n_{Fm}}$. Same as in Fig. 5 except $k_B T=0.02e^2/\epsilon l_0$. Note that $\mu_{00}(N)$ depends on the approximation.

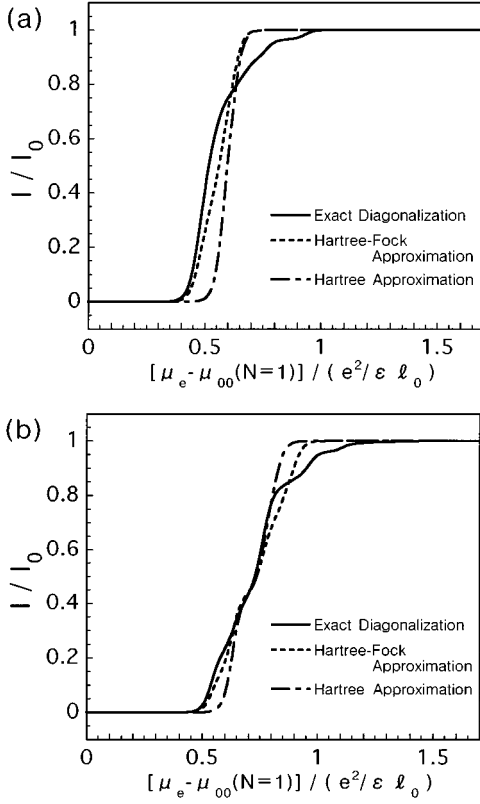


FIG. 8. Comparison with approximate calculations at $n_F=3$. Same as in Fig. 7.

the same position of the current onset as the Hartree-Fock result, but has a steeper rise due to larger degeneracy of two-electron levels. There is a discrepancy also at higher chemical potentials between the exact diagonalization and the Hartree-Fock approximation. Although the same trend remains²⁶ in Fig. 7(b), the difference between the exact diagonalization and the Hartree-Fock approximation is reduced. Similar results are obtained in $n_F=3$ as shown in Fig. 8.

The n_F dependence of the current-voltage characteristics in the exact diagonalization is summarized in Fig. 9(a) without $u_{n_F m}$ considered and in Fig. 9(b) with $u_{n_F m}$ considered. In Fig. 9(b) the chemical potential μ_e is measured from an averaged onset of current steps at $T=0$ due to the transition from $N=0$ to $N=1$, which is defined by $\mu_{av} = \sum_m u_{n_F m} / (n_F + 1)$ (note that μ_c should be lower than μ_{av} to have current steps corresponding to $N=0$ -to-1 transitions). The chemical-potential difference between the centers of $N=0$ -to-1 slope and 1-to-2 slope in the current-voltage characteristics, which corresponds to the Coulomb blockade threshold, decreases with the increase of n_F because the wave-function extent increases with n_F and the typical intralevel Coulomb interaction decreases. There is a difference in the width of the slope region between Figs. 9(a) and 9(b). In the absence of $u_{n_F m}$ [Fig. 9(a)], the slope width is again determined by the typical intralevel Coulomb interaction and decreases with the increase of n_F , whereas in Fig. 9(b) the slope region is widened by the splitting of one-electron energy levels due to $u_{n_F m}$ and its width is roughly independent of n_F .

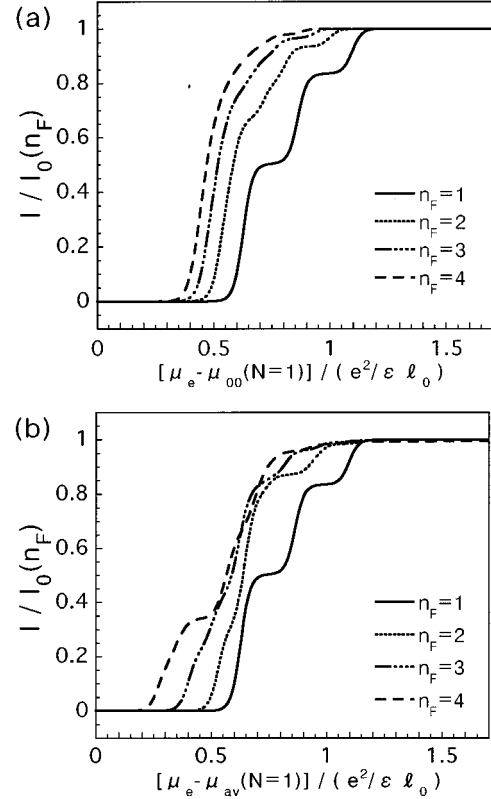


FIG. 9. n_F dependence of the current due to the transition between $N=1$ and $N+1$ electrons in the dot (a) without $u_{n_F m}$ and (b) with $u_{n_F m}$. $k_B T = 0.02 e^2 / \epsilon l_0$ and $\gamma_c / \gamma_e = 100$. Note that I_0 depends on n_F . In (b) μ_{av} is the average of $u_{n_F m}$ over one-electron states.

A remarkable dependence on N of the current-voltage characteristics is seen in Fig. 10(a) for $n_F=2$: the width of the slope region between plateaus is reduced considerably in larger N . This feature is present also in $n_F=3$. This is seen also in the result in the Hartree-Fock approximation and therefore has nothing to do with the correlation effect. This feature is explained below by the number of $(N+1)$ -electron states participating in the transport.

In the limit of large γ_c / γ_e ,

$$I = -(e/\hbar) \sum_{\alpha} P_{\alpha} \sum_{\beta} \Gamma_e(\beta|\alpha) \quad (30)$$

from Eq. (25). The current increases with the number of β states participating in the transport and is saturated to be $-(e/\hbar) \gamma_e / N_h$ at large μ_e where all β states participate in the transport. As shown in Fig. 5, the current in the case of small N increases as μ_e crosses $\mu_{\beta\alpha}$ and in most cases α is the ground state. In the case of large N , however, many excited α states are populated through the first few β states in the vicinity of the current onset, because there are many choices in producing N -electron states from $(N+1)$ -electron states by taking one electron away. Since $\mu_{\beta\alpha}$ for high-energy excited α states and for many of β states is already smaller than μ_e , transport channels from the excited α states through many β states are immediately open, giving a narrow slope region.

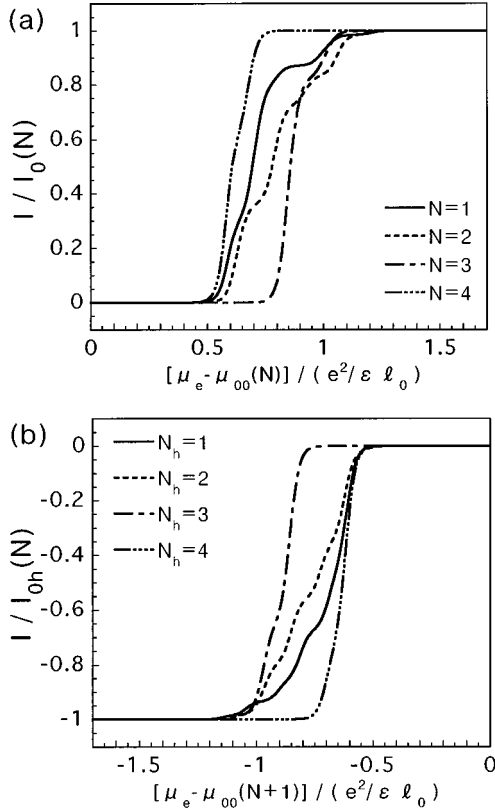


FIG. 10. (a) N dependence of the current due to the transition between N and $N+1$ electrons in the dot at $n_F=2$. $k_B T=0.02e^2/\epsilon l_0$ and $\gamma_c/\gamma_e=100$. Note that I_0 depends on N . μ_c is fixed at $\mu_{00}(N)+0.1e^2/\epsilon l_0$. (b) N_h dependence of the current due to the transition between N_h and N_h+1 holes in the dot. $N=2n_F+2-N_h$. μ_c is fixed at $\mu_{00}(N+1)-0.1e^2/\epsilon l_0$. $I_{0h}=- (e/\hbar)N\gamma_e(N_h+1)\gamma_c/[N\gamma_e+(N_h+1)\gamma_c]$.

An approximate electron-hole symmetry exists in the many-body eigenenergy distribution between N electrons and N holes in the n_F th level, although the exact electron-hole symmetry is absent because of the finite extent of the dot. This approximate electron-hole symmetry is seen in the current-voltage characteristics when the transport of a hole through the dot with N holes is compared with the transport of an electron through the dot with N electrons. An example is given in Fig. 10 when $n_F=2$. Note that in Fig. 10(b) the dependence on the hole number N_h is presented of the current due to the flow of a hole from the emitter to the collector as a function of decreasing μ_e with μ_c fixed at higher energy to keep N_h holes in the dot.

C. Linear transport

The formula of the conductance is obtained by linearizing Eq. (25) with respect to the bias voltage, which coincides with the formula already given by several authors.^{10,17,23} An important difference between the linear and nonlinear transport is that only the ground states for each N are involved in the linear transport. Examples of the conductance as a function of μ_e are presented in the linear transport. Examples of the conductance as a function of μ_e are presented in Fig. 11

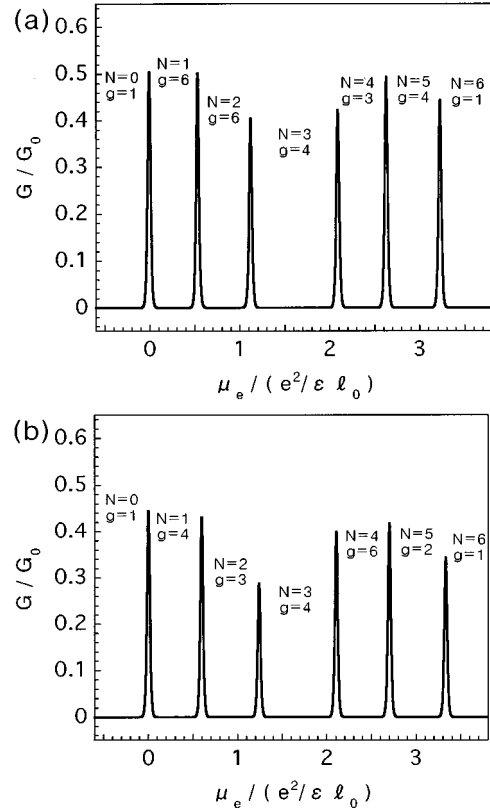


FIG. 11. Linear-response conductance G as a function of $\mu_e=\mu_c$ in the exact diagonalization at $n_F=2$ (a) without $u_{n_F m}$ and (b) with $u_{n_F m}$. $k_B T=0.01e^2/\epsilon l_0$. $G_0=(e^2/\hbar k_B T)\gamma_e\gamma_c/(\gamma_e+\gamma_c)$. μ_e is measured from the position of the first peak. g is the degeneracy of the ground states.

for $n_F=2$ and Fig. 12 for $n_F=3$. In both figures results are presented with and without $u_{n_F m}$ considered.

The peak separations are not constant, in contrast with the usual Coulomb oscillation. This clearly shows that the simple constant capacitance model is no longer valid and many-body effects play an important role. In the absence of $u_{n_F m}$ the Hund rule in the atomic physics is applicable and the ground state has spin $N/2$ below half filling due to exchange interactions. Above half filling, states with the opposite spin start to be occupied with no exchange repayment and therefore a larger peak separation is produced at half filling. This feature is retained in the presence of $u_{n_F m}$ in $n_F=2$ because of small splitting in one-electron energy levels. In $n_F=3$, however, the splitting is larger and the intra-level Coulomb interaction is smaller than in $n_F=2$. There are two groups of one-electron levels in $n_F=3$ (see Fig. 3) and the Hund rule is applicable only within each group. The third electron enters a state with the opposite spin in the lower group. In this case there are larger peak separations in $N=2, 4$, and 6 .

The peak height also varies from peak to peak and cannot be explained only by the degeneracy of many-body ground states. Here the many-body matrix element $M_{\beta\alpha} = |\langle \alpha | c_{m\sigma} | \beta \rangle|^2$ plays an important role and the correlation effect appears as in the previous study in the fractional-quantum-Hall regime.¹⁷ In particular, in $n_F=3$ and in the

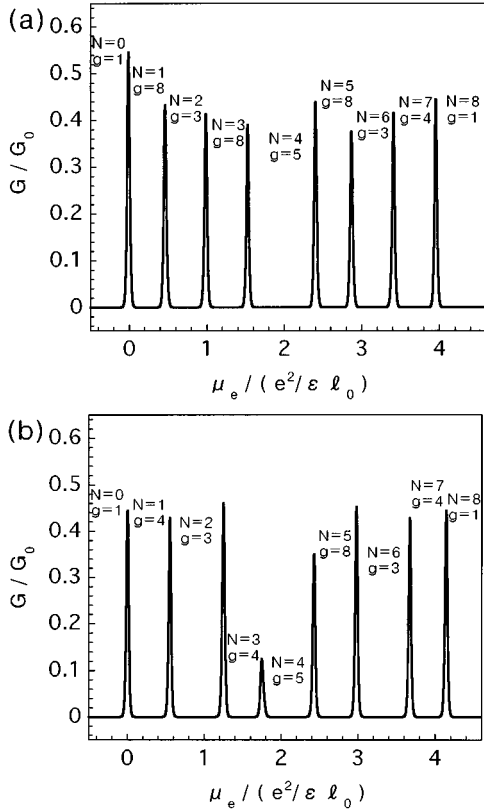


FIG. 12. Linear-response conductance G at $n_F=3$. Same as in Fig. 11.

presence of $u_{n_F m}$, the ground states have $S=1/2$ at $N=3$ and $S=2$ at $N=4$ and the transition by adding one electron is forbidden between these states because of the spin selection rule, leading to the disappearance of the corresponding conductance peak at $T=0$. The same was studied in detail for a square quantum dot in the recent theoretical work.¹⁸ In Fig. 12(b) a small peak appears between $N=3$ and $N=4$, which is due to the transition from $N=3$ excited states populated at nonzero temperatures.

D. Comparison with experiments

Many experiments³⁻⁹ have been reported on the vertical transport through a quantum dot formed in etched double-barrier resonant-tunneling structures. In most of them, however, there are no electrons in the quantum dot when the bias voltage is below the threshold. And above the threshold bias voltage, electrons begin to tunnel through the dot and the distribution of the electron number in the dot ranges from zero to the maximum value, which depends on the bias voltage. Our theory is not applicable to these cases because it assumes that the distribution of the electron number in the dot is within N and $N+1$, in which N depends on the gate voltage.

In recent experiments by Austing *et al.*⁹ the $\text{Al}_x\text{Ga}_{1-x}\text{As}$ barriers are doped selectively and there are electrons in the dot even in the absence of the bias voltage. The gate contact is attached to modify the number of electrons in the dot. Except at large bias voltages, the distribution

of the electron number in the dot is within N and $N+1$ at low temperatures, and therefore our theory is applicable to their devices. Unfortunately, however, it is shown in the Appendix that the level separation is comparable to the Coulomb interaction energy in their dots and the quantum limit assumed in our theory is not applicable in their devices, except $n_F \leq 1$.

Although their experimental results⁹ are not in the quantum limit in the whole range of the gate voltage, we here attempt to compare their experiments and our theory. Both in their results and in ours, the interval of peaks in the current as a function of the gate voltage has a tendency to decrease as the number of electrons in the dot increases (see Figs. 11 and 12) and there are considerable variations around this tendency. In the experiments, however, effects of possible bound states at impurities⁵ may be important in considering the variations in the peak spacings. Because of this and the quantum limit assumed in our theory, it is not possible in the present stage to compare the interesting features in peak intervals between their experiments and our theory.

Since it is assumed that the thermal energy $k_B T$ is much larger than the level broadening due to tunneling in our theory, peak widths are proportional to T and peak heights are proportional to $1/T$. Experimental results also show such a tendency at high temperatures, whereas the peak width is independent of the temperature at low temperatures and varies from peak to peak.⁹ It was found in another experiment¹⁹ that the height of a peak is very small at low temperatures and increases remarkably with the temperature. The mechanism due to the spin-selection rule was proposed to explain this phenomenon on the basis of numerical calculations of a square dot.¹⁸ As mentioned in the previous subsection, such a suppression of a peak at low temperatures is also found in our calculation for a circular dot.

V. CONCLUSION

We have made a theoretical study of the coherent tunneling through the quantum dot fabricated recently in semiconductor double-barrier structures, based on calculated many-body eigenstates in the dot. We have derived a current formula in the nonlinear regime in the limit of small level broadening, which coincides with the formula derived from the master equation. We have chosen the quantum limit of large separations between degenerate levels in order to get rid of complicated effects of the mixings between different levels. The quantum limit was shown to be useful in clarifying features such as the electron-hole symmetry and the strong dependence on the electron number. In most of our calculations we have assumed an asymmetric device geometry such that the dot is approximately in equilibrium with the collector, which is appropriate in extracting the whole many-body energy spectrum from the current-voltage characteristics.

Effects of the exchange and correlation appear in the current-voltage characteristics in the form of divided steps in the Coulomb staircase. Since the correlation effect is reduced by the nonuniform potential produced by filled and inert levels below the chemical potential, most of the features are well described by the Hartree-Fock approximation contrary to our expectation. This means that the features clarified in

this paper are approximately the case even when the quantum limit is not applicable. The linear conductance is shown to exhibit clearer correlation effects than the nonlinear current profile, such as the Hund rule and the spin selection rule.

Observed current-voltage characteristics exhibit much richer structures. To clarify such discrepancies between the experiment and the theory, it is necessary to perform a microscopic calculation of electron states that takes account of the detailed device structure, such as the barrier shape in the presence of the bias and the subband structure in leads.

ACKNOWLEDGMENTS

The authors would like to thank T. Ando, S. Tarucha, and N. Tokuda for valuable discussions. This work was supported in part by the Grant-in-Aid for Scientific Research on Priority Area “computational Physics as a New Frontier in Condensed Matter Research” from the Ministry of Education, Science and Culture, Japan and in part of the Visiting Researcher’s Program of the Institute for Solid State Physics, the University of Tokyo. Numerical calculations were performed at Hokkaido University Computing Center.

APPENDIX: APPLICABILITY OF THE QUANTUM LIMIT

Here we discuss the applicability of the approximation to neglect the level mixing due to off-diagonal Coulomb matrix elements, by considering the contribution to the level mixing of the Hartree-Fock potential due to the electrons below the n_F th level, which is the most dominant effect to mix harmonic-oscillator states with different n . We also discuss a possibility of the level crossing and show that it is less probable. We write the condition in terms of the impurity density and the effective mass as well as in terms of $e^2/\epsilon l_0$ and $\hbar\omega_0$, and show that the quantum limit may be applicable if the semiconductor with smaller effective mass is used in the quantum well and the impurity density is the same as in the recent experiment on the GaAs dot.⁹

The one-electron part of the Hamiltonian including effects of the Hartree-Fock potential due to the electrons below the n_F th level, is expressed by

$$H_d(1e) = \sum_{nm\sigma} \epsilon_n c_{nm\sigma}^\dagger c_{nm\sigma} + \sum_{nn'm\sigma} u_{nn',m}(n_F) c_{nm\sigma}^\dagger c_{n'm\sigma}, \quad (\text{A1})$$

with

$$u_{nn',m}(n_F) = \sum_{n'' < n_F, m''} (2U_{nmn''m''n'm''n''m} - U_{nmn''m''n'm''m''}). \quad (\text{A2})$$

The measure of the level mixing is $|u_{nn',m}(n_F)/(\epsilon_n - \epsilon_{n_F})|$ for the electron in the n_F th level and its square is the first-order probability of finding the electron in the state n . If this is much smaller than unity, the level mixing can be neglected. Note that n is an integer to satisfy that $n - n_F$ is even from the conservation of m in the circular dot. Since it depends strongly on n_F , we estimate the measure of the level

mixing for each fixed n_F . Its maximum value for each fixed n_F and any possible n and m is written as

$$\max \left(\left| \frac{u_{nn',m}(n_F)}{\epsilon_n - \epsilon_{n_F}} \right| \right) = \alpha \frac{(e^2/\epsilon l_0)}{\hbar\omega_0}, \quad (\text{A3})$$

where $\alpha=0.19$ for $n_F=1$, $\alpha=0.51$ for $n_F=2$, and $\alpha=0.85$ for $n_F=3$, respectively.

The quantum limit also fails if the n_F th level crosses the lower level or the higher level due to $u_{nn',m}(n_F)$. The condition for no level crossing is that the highest one-electron level with n_F is lower than the lowest one with n_F+1 and the lowest one-electron level with n_F is higher than the highest one with n_F-1 . This condition is written as $\beta(e^2/\epsilon l_0)/\hbar\omega_0 < 1$. The value of β is calculated to be $\beta=0.20$ for $n_F=1$, $\beta=0.54$ for $n_F=2$ and $\beta=0.81$ for $n_F=3$, respectively. Therefore no level crossing takes place if the level mixing is negligible.

In the recent experiment,⁹ the Coulomb energy between two electrons is estimated to be 9 meV when the number of electrons in the dot is two from the zero-current plateau in the current-voltage characteristics in the Coulomb-blockade regime. If the level mixing is neglected in this case, the corresponding energy is calculated to be $1.25e^2/\epsilon l_0$. From these estimations it is deduced that $e^2/\epsilon l_0=7.2$ meV, from which $\hbar\omega_0=4.9$ meV and $(e^2/\epsilon l_0)/\hbar\omega_0=1.45$. This means that the experimental result is not in the quantum limit, except $n_F \leq 1$.

From this, however, we can derive a semiempirical formula for $(e^2/\epsilon l_0)/\hbar\omega_0$ to know in which devices the quantum limit is applicable. First we assume a homogeneous ionized-impurity density N_D over the whole device. Then $\hbar\omega_0$ and $e^2/\epsilon l_0$ are given by $\hbar\omega_0=(2\pi e^2 \hbar^2 N_D/m^* \epsilon)^{1/2}$ and $e^2/\epsilon l_0=(m^* \omega_0/\hbar)^{1/2} e^2/\epsilon$, respectively. Therefore the ratio of the two is given by

$$\frac{e^2/\epsilon l_0}{\hbar\omega_0} = \left(\frac{1}{2\pi a_B^3} \right)^{1/4} \left(\frac{m^*/m_0}{\epsilon} \right)^{3/4} N_D^{-1/4}, \quad (\text{A4})$$

with a_B the Bohr radius and m_0 the free-electron mass. Next we consider effects of the inhomogeneous distribution of ionized impurities in the experiments.⁹ In the experiments the confinement potential parallel to the interface is formed by δ -doped ionized impurities with the sheet density N_s in $\text{Al}_x\text{Ga}_{1-x}\text{As}$ barriers. Here, for simplicity, we assume that the ratio of $e^2/\epsilon l_0$ to $\hbar\omega_0$ has the same dependence on the impurity density as the ratio in the homogeneous case has. Then the prefactor is found from the experimental values⁹ of $N_s=2.0 \times 10^{11} \text{ cm}^{-2}$ and $e^2/\epsilon l_0=7.2$ meV and from $m^*=0.066m_0$ and $\epsilon=13.13$ for GaAs. Finally the condition for the quantum limit to be applicable is written as

$$\alpha \frac{e^2/\epsilon l_0}{\hbar\omega_0} = 91.16 \alpha \left(\frac{m^*}{\epsilon} \right)^{3/4} N_s^{-1/4} \ll 1, \quad (\text{A5})$$

where N_s is in units of 10^{11} cm^{-2} . This shows that it is easier to satisfy the quantum limit in semiconductors with smaller effective mass. For example, $(e^2/\epsilon l_0)/\hbar\omega_0$ is 0.3 in InSb well and 0.7 in InAs well in the same impurity density of $N_s=2.0 \times 10^{11} \text{ cm}^{-2}$.

- ¹M. A. Kastner, Phys. Today **46** (1), 24 (1993); Rev. Mod. Phys. **64**, 849 (1992).
- ²D. V. Averin and K. K. Likharev, in *Mesoscopic Phenomena in Solids*, edited by B. L. Altshuler *et al.* (Elsevier, Amsterdam, 1991), p. 173.
- ³M. A. Reed *et al.*, Phys. Rev. Lett. **60**, 535 (1988).
- ⁴B. Su *et al.*, Phys. Rev. B **46**, 7644 (1992).
- ⁵M. W. Dellow *et al.*, Phys. Rev. Lett. **68**, 1754 (1992).
- ⁶P. Guéret *et al.*, Phys. Rev. Lett. **68**, 1896 (1992).
- ⁷M. Tewordt *et al.*, Phys. Rev. B **45**, 14 407 (1992).
- ⁸S. Tarucha *et al.*, Surf. Sci. **305**, 547 (1994).
- ⁹D. G. Austing *et al.*, Jpn. J. Phys. **34**, 1320 (1995); Semicond. Sci. Technol. (to be published); (unpublished).
- ¹⁰C. W. J. Beenakker, Phys. Rev. B **44**, 1646 (1991).
- ¹¹D. V. Averin *et al.*, Phys. Rev. B **44**, 6199 (1991).
- ¹²P. L. McEuen *et al.*, Phys. Rev. B **45**, 11 419 (1992).
- ¹³M. Stopa, Phys. Rev. B **48**, 18 340 (1993).
- ¹⁴N. F. Johnson and M. C. Payne, Phys. Rev. B **45**, 3819 (1992).
- ¹⁵P. Hawrylak, Phys. Rev. Lett. **71**, 3347 (1993).
- ¹⁶S.-R. Eric Yang *et al.*, Phys. Rev. Lett. **71**, 3194 (1993).
- ¹⁷J. M. Kinaret *et al.*, Phys. Rev. B **45**, 9489 (1992); **46**, 4681 (1992).
- ¹⁸D. Weinmann, W. Häusler, and B. Kramer, Phys. Rev. Lett. **74**, 984 (1995).
- ¹⁹J. T. Nicolls *et al.*, Phys. Rev. B **48**, 8866 (1993).
- ²⁰L. I. Glazman and M. É. Raïkh, Pis'ma Zh. Éksp. Teor. Fiz. **47**, 378 (1988) [JETP Lett. **47**, 452 (1988)].
- ²¹T. K. Ng and P. A. Lee, Phys. Rev. Lett. **61**, 1768 (1988).
- ²²H. Akera, Phys. Rev. B **47**, 6835 (1993). The formulation developed in this paper for the interference out of resonance needs to be modified to study the interference in the resonant tunneling.
- ²³Y. Meir and N. Wingreen, Phys. Rev. Lett. **68**, 2512 (1992).
- ²⁴The summation over states j is essentially the summation over unoccupied levels in leads of the state i . The distribution of electrons in each i is replaced by the Fermi distribution since it is assumed that the number of levels in each lead within their level broadening is large and its statistical fluctuation is negligible.
- ²⁵This simple relation is exact in the limit of large γ_c/γ_e . Since P_α and $\mu_{\beta\alpha}$ are independent of α in the absence of $u_{n_{fm}}$, Eq. (30) becomes $I = -(e/\hbar)\gamma_e(N+1)P_\alpha\sum_{\beta}f_e(\mu_{\beta\alpha})$, giving a sum of step functions at $T=0$.
- ²⁶A discrepancy between the Hartree-Fock and the Hartree approximations appears at higher chemical potentials in Fig. 7(b), but this is only due to the difference in the single-particle energy splitting between the two approximations (see the caption of Fig. 3) and is not important.